Available online at www.sciencedirect.com
SCIENCE DIRECT®
Journal of Power Sources 119–121 (2003) 247–251
JOURNAL OF POWER SOURCES
www.elsevier.com/locate/jpowsour

Fine-particle lithium iron phosphate $LiFePO_4$ synthesized by a new low-cost aqueous precipitation technique

G. Arnold, J. Garche, R. Hemmer, S. Ströbele, C. Vogler, M. Wohlfahrt-Mehrens*

Center for Solar Energy and Hydrogen Research, Baden-Württemberg Division 3, Electrochemical Energy Storage and Conversion Helmholtzstraße 8, Ulm D-89081, Germany

Abstract

Phase pure, homogeneous, and well-crystallized lithium iron phosphate $LiFePO_4$ was synthesized by aqueous co-precipitation of an Fe(II) precursor material and succeeding heat treatment in nitrogen. The particle morphology of the precursor is preserved during the heat treatments. Excellent electrochemical properties in terms of capacity, reversibility, cycling stability and rate capability have been achieved. The thermal stability of charged electrodes is superior versus other positive electrode materials. If reductive synthesis conditions are used in the heat treatments, problems arise from the possible generation of iron phosphide.

Keywords: $LiFePO_4$; Fe(II); X-ray diffraction

1. Introduction

Lithium iron phosphate $LiFePO_4$ is an interesting alternative positive electrode material for lithium and lithium-ion batteries. It has advantages in terms of environmental benignity, potential low-cost synthesis, cycling stability, and high temperature capability. Main problem is the poor rate capability [1,2]. Improvements of rate capability have been achieved by synthesizing small particles [3] and by an electronic conductive particle coating [4,5]. Aqueous precipitation techniques are very suitable for the synthesis of small particles. Techniques of this kind, described so far, are based on precursors containing Fe(III) and require an electrochemical [6] or chemical reduction step [7]. In this work, a new low-cost and environmental benign aqueous precipitation technique is presented, which affords no reduction step.

2. Experimental procedures

2.1. Synthesis procedure

A finely dispersed precursor containing stoichiometric composite of Fe(II) phosphate and lithium phosphate, lithium and phosphate compounds is co-precipitated by addition and stirring of appropriate aqueous solutions of the respective salts under pH control. The precipitate is filtrated, washed several times with distilled water, and dried. These process steps are all performed under a nitrogen atmosphere in order to exclude oxygen. The dried precursors are heat treated for 12 h at temperatures ranging from 650 to 800 °C in a nitrogen flow. Details of this procedure are published elsewhere [8].

2.2. Structural and morpholgical characterization

X-ray diffraction (XRD) profiles of the samples were measured with a Siemens D5000 diffractometer (Cu Kα radiation). Structural parameters were determined by Rietveld analysis of diffraction profiles, using the Bruker AXS program Win-Rietveld. The space group setting was *Pnma*. As starting values for the orthorhombic lattice constants and as atomic site parameters the single crystal values for the mineral triphylite of Streltsov and Belokonova [9] were used. For simplification, the site occupation ratios were set to 1. Only the lattice constants, the scale factor and the profile parameters were refined, since atomic site parameters from single crystal diffraction are more reliable. The impurity phase lithium-*ortho*-phosphate Li_3PO_4 was also included in the refinements, but only the scale factor was refined and all structural parameters were held fixed to the single crystal values of Zemann [10]. The crystallite size of the lithium iron phosphate was calculated by the Scherrer

* Corresponding author. Tel.: +49-731-9530-601; fax: +49-731-9530-666.
E-mail address: margret.wohlfahrt-mehrens@zsw-bw.de (M. Wohlfahrt-Mehrens).

0378-7753/03/$ – see front matter
doi:10.1016/S0378-7753(03)00241-6

equation $\sigma = \lambda/(\beta_{2\theta} \times \cos\theta)$ from the integral breadth β of the seven strongest, well-resolved reflection peaks. The β values were determined by profile analysis. Since no anisotropic reflection broadening could be found in the diffraction profiles, an isometric crystallite shape was assumed and the median of the calculated crystallite size values was taken in each case. SEM images were recorded by a LEO 1530 VP, equipped with a field emission electrode. The particle size distribution was determined by a SYSMEX FPIA-2100 optical particle size analyzer.

2.3. Electrochemical characterization

For electrode preparation, 20 wt.% of conductive carbon and 10 wt.% of PTFE powder were added to the lithium iron phosphate powder and mixed in an agate mortar, rolled into flakes, and pressed into strips of aluminum grid. Each strip was mounted as positive electrode versus counter and reference electrodes of lithium metal in a glass cell, and filled with a liquid electrolyte (Merck LP30, i.e. 1 M $LiPF_6$ in EC:DMC = 1:1). Assemblage of the cells and electrochemical measurements were performed in an argon box. The cells were galvanostaticaly cycled at room temperature between 2.9 and 4.0 V versus Li/Li^+ at a specific current of *C*/20.

2.4. Thermal measurements of charged cathodes

Charged cells were disassembled in an argon box. The positive electrodes were washed in DMC, dried overnight, and sealed in punctured aluminum cans, for simultaneous thermal analysis (STA). In this method, differential scanning calorimetry (DSC) and thermal gravimetry (TG) are applied simultaneously to the sample, allowing a simultaneous measurement of changes in enthalpy and weight. The thermal scans were performed with a heating rate of 10 K/min up to a temperature of 400 °C in an argon stream.

3. Results and discussion

3.1. Structural results

Fig. 1 presents the X-ray diffraction pattern of a typical sample, synthesized by the new process. All diffraction lines can be attributed to the orthorhombic olivine type phase $LiFePO_4$ and to a minor impurity phase, which is lithium-*ortho*-phosphate Li_3PO_4. Additionally, the profiles of the reflection peaks are quite narrow and symmetric. Thereby, a nearly phase pure homogeneous and well-crystallized product is indicated.

A series of samples was synthesized by calcination of one co-precipitated precursor at various synthesis temperatures. In Fig. 2, the volume of the rhombic unit cell and the relative lattice parameters of these materials are plotted versus the synthesis temperature. The relative lattice parameters are normalized to the respective values of the sample synthesized at 650 °C, in order to visualize the temperature dependency more clearly. The absolute lattice parameters for this reference material are $a = 10.323$ Å, $b = 6.003$ Å, $c = 4.694$ Å. The cell volume and the lattice parameters a and c decrease slightly with increased synthesis temperature, whereas the lattice parameter b is unaffected. Obviously, there is a shrinkage of the crystal structure within the crystallographic a–c plane for an increased synthesis temperature. This result may indicate the existence of an unidentified stoichiometric or structural deviation from the ideal olivine type $LiFePO_4$, which depends on the synthesis temperature.

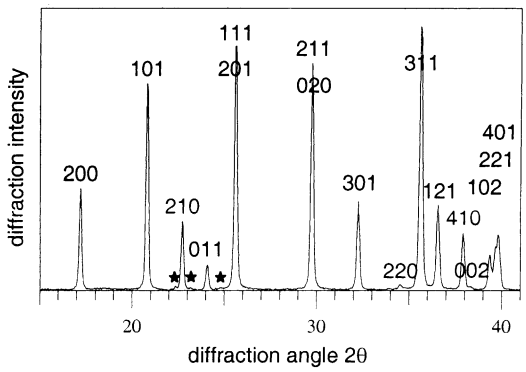

Fig. 1. X-ray diffraction pattern of lithium iron phosphate, synthesized by aqueous co-precipitation of an Fe(II) precursor and heat treatment in nitrogen. The reflection peaks of the olivine phase $LiFePO_4$ are signed by their Miller indices in space group *Pnma*. The asterisks sign reflection peaks of lithium-*ortho*-phosphate Li_3PO_4 as minor impurity phase.

3.2. Morphological results

Fig. 3 shows the SEM images of a co-precipitated precursor material and the corresponding end product, obtained after heat treatment in nitrogen. Both powders consist of

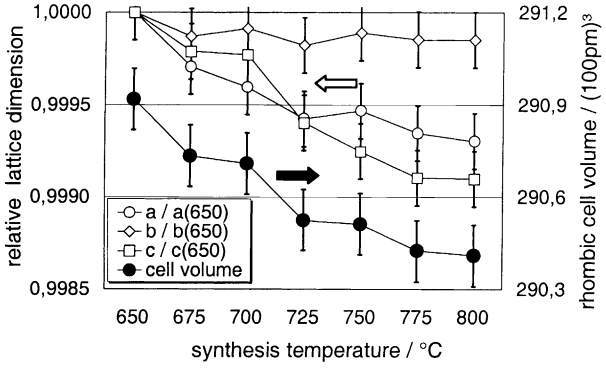

Fig. 2. Influence of the synthesis temperature on rhombic cell volume and relative lattice parameters of different samples, synthesized from one precursor at various synthesis temperatures. For clarity, the lattice constants are normalized to the respective values for the material synthesized at 600 °C. The absolute values for this reference material are $a = 10.323$ Å, $b = 6,003$ Å, $c = 4,694$ Å.

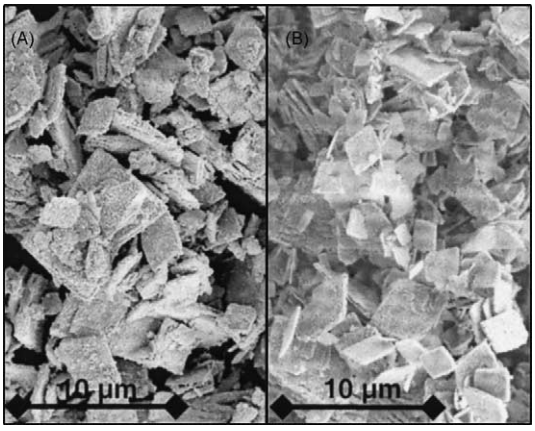

Fig. 3. SEM images of an Fe(II) precursor, co-precipitated from aqueous solutions (A) and of lithium iron phosphate, synthesized thereof by heat treatment in nitrogen (B).

dispersed, flat, rhombus shaped particles. Therefore, the particle morphology of the co-precipitated precursors is preserved during the heat treatment. The flat $LiFePO_4$ particles consist of small isometric crystallites in the nanometer range, as a close inspection of the SEM image and the determination of the Scherrer crystallite size reveal. Fig. 4 compares the influence of the synthesis temperature on volume based particle size distribution and Scherrer crystallite size for a sample series, derived from one precursor material. The Scherrer crystallite size is much smaller than the particle size in each case and increases for increased synthesis temperature, due to enhanced crystal growth. The volume based particle size distribution is represented by the diameters of D10, D50 and D90 values determined by optical particle size analyzer. The particle size distribution is not significantly influenced by the synthesis temperature, because it is determined by the precursor material and preserved during the heat treatment. Since extremely fine (<1 μm) and extremely course (>20 μm) particle fractions are absent, the materials are suitable for usual electrode preparation techniques.

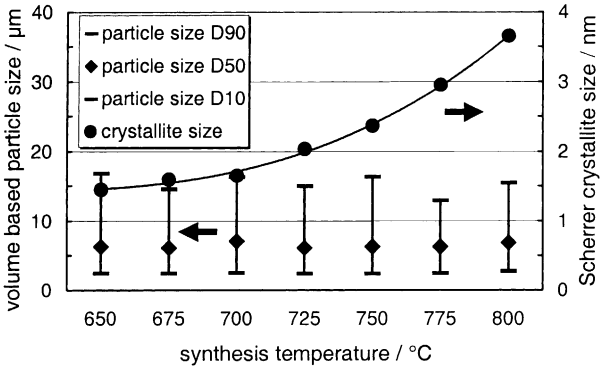

Fig. 4. Influence of the synthesis temperature on crystallite size and particle size distribution of different samples, synthesized from one precursor at various synthesis temperatures.

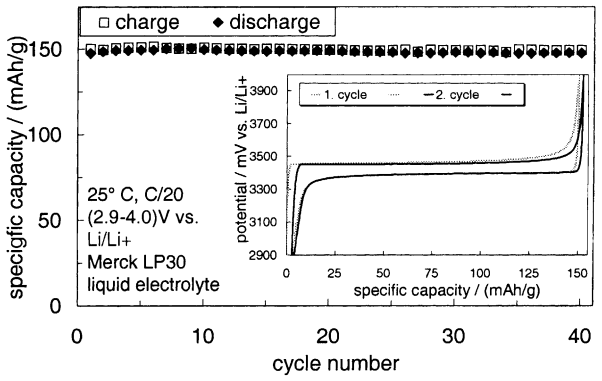

Fig. 5. Cycling test of lithium iron phosphate, synthesized by the new process and potential capacity diagram of the first two cycles.

3.3. Electrochemical results

Fig. 5 depicts the specific charge and discharge capacities of a cycling test. A discharge capacity of 150 mAh/g (theoretical value: 170 mAh/g), accompanied by a high reversibility, even in the first cycle, and a good cycling stability are obtained. The corresponding potential capacity diagram for the first two cycles shows the typical flat potential plateau at 3.4 V versus Li/Li^+, resulting from the phase transition of triphylite $LiFePO_4$ to heterosite $FePO_4$ [1]. Also, a comparatively small polarization is obtained. Fig. 6 compiles the results of a discharge rate capability test. At a specific current of *C*/20, a discharge capacity of 160 mAh/g is achieved and at *C*/2 the discharge capacity is still higher than 145 mAh/g. Therefore, the materials offer a comparatively good rate capability.

3.4. Results of thermal measurements

The thermal decomposition of many delithiated positive electrode materials, often accompanied by oxygen evolution, is a well known problem [11,12]. But delithiated lithium iron phosphate is reported to be comparatively stable [1]. In this study, electrodes of a lithium iron phosphate

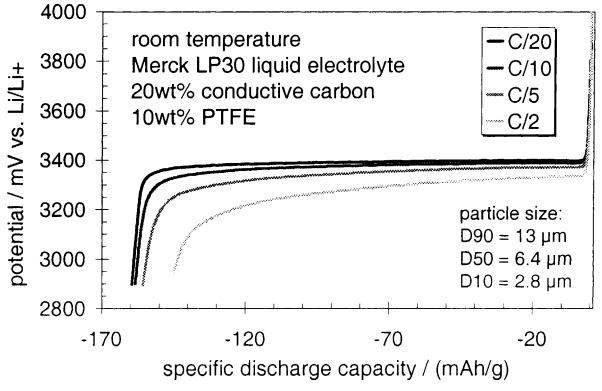

Fig. 6. Rate capability test of lithium iron phosphate, synthesized by the new process.

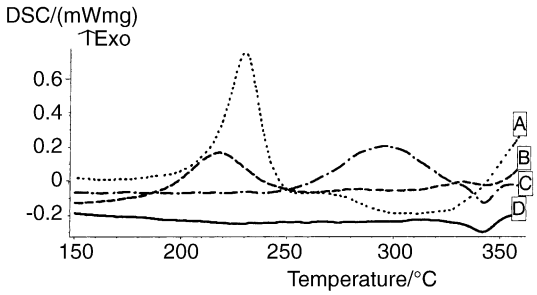

Fig. 7. DSC scans of positive electrode materials in the charged state, measured without electrolyte. (A) $Li_{0.2}Ni_{0.8}Co_{0.15}Al_{0.05}O_2$; (B) $Li_{0.5}CoO_2$; (C) $Li_{0.15}Mn_2O_4$; (D) "$Li_{0.1}FePO_4$".

sample, synthesized by the new process, and of three other positive electrode materials were charged and thermally analyzed. For that, electrodes of a Co/Al doped lithium nickel oxide, a lithium cobalt oxide, and a lithium manganese spinel were potentiostaticly charged at 4.3 V versus Li/Li^+. Whereas the lithium iron phosphate electrode was galvanostaticaly charged to a delithiation degree of 90%, since the state of charge of a two-phase system is defined more usefully by that way. The delithiation degrees of the other tested materials are calculated from the electric charge, flown in each charge process and are specified in the figures. Figs. 7 and 8 compare the DSC and TG curves measured simultaneously for the four kinds of electrodes. The delithiated lithium nickel oxide shows the most vehement exothermic reaction at a temperature beneath 250 °C, followed by a large weight loss, due to oxygen evolution. The charged lithium cobalt oxide electrode also reacts at such low temperatures, but with less reaction enthalpy and oxygen evolution. The exothermic reaction of the delithiated lithium manganese spinel starts at a much higher temperature and there is no weight loss up to 400 °C. The delithiated lithium iron phosphate however, shows no exothermic reaction and no weight loss up to 400 °C, at all.

3.5. Phosphide generation under reductive conditions

A slightly oxidized Fe(II) precursor material, obtained by short exposure to the air for 30 min, was heat treated under various reductive reaction conditions, which were ensured by addition of defined amounts of hydrogen to the nitrogen flow or by addition of carbon to the precursor. The degree of oxidation after the heat treatments was estimated by the color of the samples, which turns from white, via beige, to a slightly reddish brown. This is a very sensitive visual indicator for Fe(III), because a distinct change of color is already visible, even if no Fe(III) impurity phase can be detected by X-ray diffraction, yet. According to our experience, the color of the powders is a very sensitive, semi-quantitative indicator for Fe(III) and is a simple visual quality criterion for the products. This criterion was used, because quantitative methods for Fe(III) determination like redox titration or Moessbauer spectroscopy were not available within this work. In most of the reductive synthesis experiments, the iron phosphide phase barringerite Fe_2P was generated by reduction of phosphate and iron. The occurrence of this phase, even in traces, leads to a characteristic light or dark gray color of the powders. In Fig. 9, the segments of XRD spectra, characteristic for the occurrence of barringerite, are compared for the products of some reductive synthesis experiments. If the slightly oxidized Fe(II) precursor is heat treated in nitrogen in absence of any reductive additive (profile E), a light brown color indicates a considerable content of Fe(III), though no distinct Fe(III) phase could be detected. If the same precursor is heat treated in nitrogen, containing 1 vol.% of hydrogen, no phosphide generation can be detected (profile D). But the light beige color of the sample indicates traces of remaining Fe(III), due to an incomplete reduction. If a precursor, containing carbon as reductive additive, is heat treated in pure nitrogen, also no phosphide could be detected by XRD (profile C). However, the carbon content gives this powder a black color and allows no visual estimation of a remaining Fe(III) content. If a carbon-free precursor material is heat treated under a nitrogen flow, containing 10 vol.% of

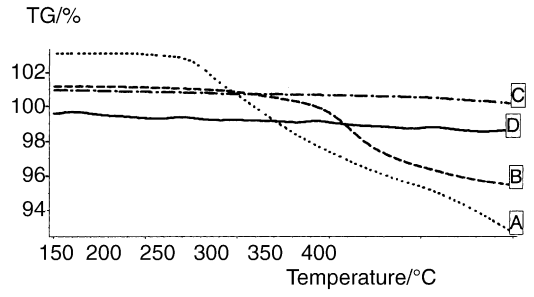

Fig. 8. TG scans of positive electrode materials in the charged state, measured without electrolyte. (A) $Li_{0.2}Ni_{0.8}Co_{0.15}Al_{0.05}O_2$; (B) $Li_{0.5}CoO_2$; (C) $Li_{0.15}Mn_2O_4$; (D) "$Li_{0.1}FePO_4$".

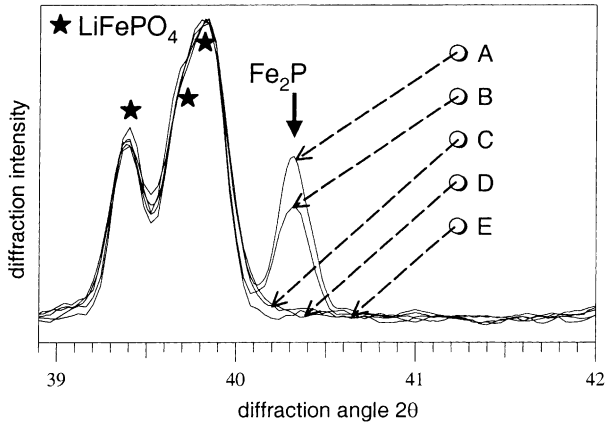

Fig. 9. XRD patterns of samples, synthesized from a slightly oxidized Fe(II) precursor by various reductive heat treatments. (A) 10 vol.% H_2 in N_2/5 wt.% carbon/black color; (B) 10 vol.% H_2 in N_2/dark gray color; (C) pure N_2/5 wt.% carbon/black color; (D) 1 vol.% H2 in N2/light beige color; (E) pure N2/light brown color.

hydrogen, a considerable amount of iron phosphide is generated (profile B). If the precursor additionally contains carbon, this amount is even increased (profile A). In conclusion, it is difficult, to find reductive conditions, which allow the complete reduction of even small impurities of Fe(III) in the precursor, without generation of a phosphide phase.

4. Conclusion

Phase pure, homogeneous, and well-crystallized lithium iron phosphate $LiFePO_4$ can be synthesized by aqueous co-precipitation of an Fe(II) precursor material and succeeding heat treatment in nitrogen. An influence of the synthesis temperature on the crystallographic lattice parameters may indicate the existence of an unidentified temperature dependent deviation from the ideal structure or stoichiometry. The particle morphology of the precursor is preserved during the heat treatments. Excellent electrochemical properties in concerns of capacity, reversibility, cycling stability and rate capability are achieved. The thermal stability of charged electrodes is superior to other positive electrode materials. If reductive synthesis conditions are used in the heat treatments, problems arise from the possible generation of iron phosphide due to phosphate reduction.

References

[1] A.K. Padhi, K.S. Nanjundaswamy, J.B. Goodenough, J. Electrochem. Soc. 144 (1997) 1188.
[2] A.S. Andersson, L. Häggström, B. Kalska, J.O. Thomas, Electrochem. Solid-State Lett. 3 (2000) 66.
[3] A. Yamada, S.C. Chung, K. Hinokuma, J. Electrochem. Soc. 148 (2001) A224.
[4] N. Ravet, J.B. Goodenough, S. Besner, M. Simoneau, P. Hovington, M. Armand in: Proceedings of the 196th ECS Meeting, Honolulu, October 1999.
[5] N. Ravet, Y. Chouninard, J.F. Magnan, S. Besner, M. Gauthier, M. Armand, J. Power Sources 97–98 (2001) 503.
[6] P.P. Prosini, in: Proceeding of the ECS Fall Meeting, San Francisco, USA, October 2001.
[7] C. Masquelier, in: Proceedings of the Eighth Euroconference on Ionics, Carvoeiro, Portugal, September 2001.
[8] WO 02/083555 A2.
[9] V.A. Streltsov, E.L. Belokonova et al., Acta Cryst. B 49 (1993) 147.
[10] J. Zemann, Acta Cryst. 13 (1960) 863.
[11] T. Ohzuku, A. Ueda, M. Kouguchi, J. Electrochem. Soc. 142 (1995) 4033.
[12] Z. Zhang, D. Fouchard, J.R. Rea, J. Power Sources 70 (1998) 16.